The Meteoritical Society

Meteoritics & Planetary Science 56, Nr 2, 352–361 (2021)
doi: 10.1111/maps.13622

Extension of the plasma radiation database PARADE for the analysis of meteor spectra

Stefan LOEHLE[1]*, Martin EBERHART[1], Fabian ZANDER[1], Arne MEINDL[1], Regina RUDAWSKA[2], Detlef KOSCHNY[2], Joe ZENDER[2], Ron DANTOWITZ[3], and Peter JENNISKENS[4]

[1]Institut für Raumfahrtsysteme, Universität Stuttgart, Stuttgart 70569, Germany
[2]ESA ESTEC, Noordwijk 2201, The Netherlands
[3]Dexter Southfield, Boston, MA02445, Massachusetts, USA
[4]SETI Institute, Mountain View, CA94043, California, USA
*Corresponding author. Email: loehle@irs.uni-stuttgart.de

(Received 21 February 2018; revision accepted 22 November 2020)

Abstract–The advancement in the acquisition of spectral data from meteors, as well as the capability to analyze meteoritic entries in ground testing facilities, requires the assessment of the performance of software tools for the simulation of spectra for different species. The Plasma Radiation Database, PARADE, is a line-by-line emission calculation tool. This article presents the extensions implemented for the simulation of meteor entries with the additional atomic species Na, K, Ti, V, Cr, Mn, Fe, Ca, Ni, Co, Mg, Si, and Li. These atoms are simulated and compared to ground testing spectra and to observed spectra from the CILBO observatory. The diatomic molecules AlO and TiO have now been added to the PARADE database. The molecule implementations have been compared to the results of a simple analytical program designed to approximate the vibrational band emission of diatomic molecules. AlO and TiO have been identified during the airborne observation campaigns of re-entering man-made objects WT1190F and CYGNUS OA6. Comparisons are provided showing reasonable agreement between observation and simulation.

INTRODUCTION

The observation of a meteor in Earth's atmosphere is probably one of the oldest astronomical observations (Oepik 1958). The impressive glowing trail of a shooting star is actually the physical process of an atmospheric entry of interplanetary rocks.

The first photograph of a meteor spectrum was taken coincidentally in 1897 (Ceplecha et al. 1998). Meteor spectroscopy became of higher scientific interest in the 20th century with the advent of useful prism photographic systems and extensive studies of meteor spectra started in the second half of the 20th century when transmission gratings became available (Millman 1932) and the acquisition of higher resolution photographic spectra was developed. The basic application is that the spectral analysis allows the identification of meteoritic composition and eventually that of the parent body in space (Ceplecha et al. 1998; Jenniskens 2006).

There are a number of meteor observation systems in operation (Colas et al. 2015; Jenniskens 2017). The European Space Agency (ESA) maintains a double station meteor camera system on the Canary Islands (Koschny et al. 2013). The system, called CILBO (Canary Island Long-Baseline Observatory), consists of an intensified video camera on two islands (La Palma and Tenerife) and one additional camera on Tenerife for spectral data acquisition using a 600 L mm^{-1} transmission grating in a slitless configuration for the wavelength interval from 400 to 800 nm. This third camera is aligned in a way that the video camera and the spectral camera observe the same object, the video camera captures images, and the spectral camera acquires the first-order spectral data. Figure 1 shows an example measurement. The two top images are

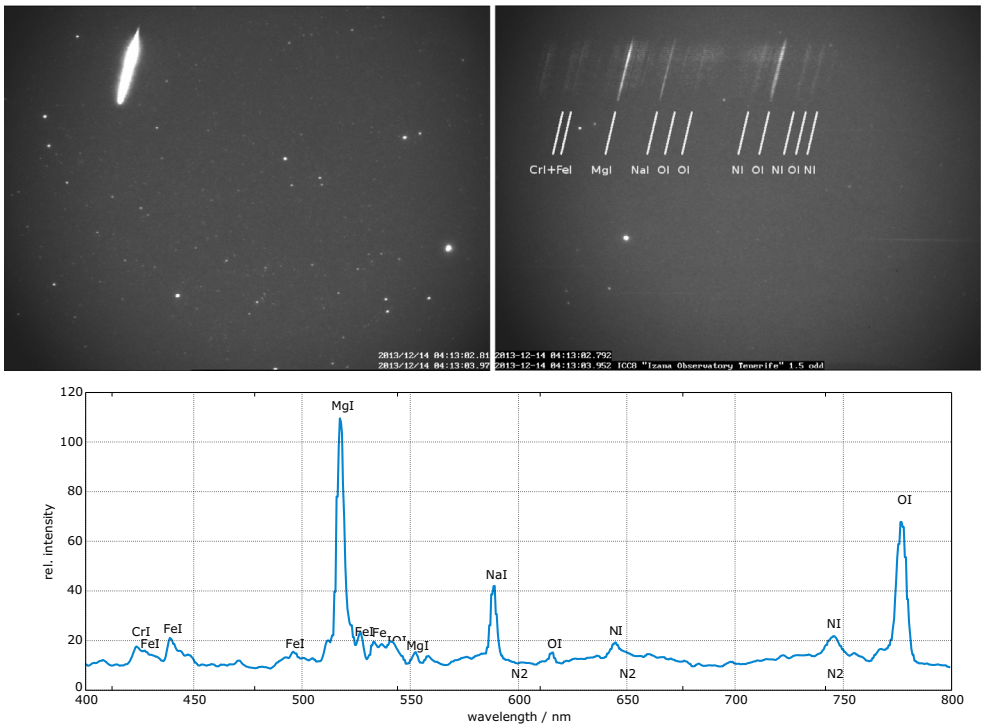

Fig. 1. Exemplary data recorded with CILBO (top left: single frame of camera ICC8, top right: single frame of camera ICC7 of the same event, bottom: spectra from ICC8 camera). (Color figure can be viewed at wileyonlinelibrary.com.)

composites of stacked frames of the same event from the two intensified cameras ICC7 (left) and ICC8 (right, with spectra). A spectral raw image can be seen on the top right. Analyzing these data results in the spectrum at the bottom of the figure. The shown bottom spectrum is integrated over the duration of the event. Prominent atomic line emission and the molecular band radiation of N2 are indicated. With an appropriate radiation simulation code, this spectrum can be investigated, atomic and molecular lines can be identified, and the atmospheric entry can be analyzed; for example, temperatures and ablation processes can be identified if the temporal behavior of an emission line were considered, too (upper right figure). The requirement to simulate meteor spectra was the motivation for the extension of the European Plasma Radiation Database (PARADE) presented in this study. Recently, a collection of measured meteor spectra was published by Vojáček et al. (2015). The various meteors observed are mainly characterized by the appearance of prominent atomic emission lines of Mg, Na, and Fe. The identification of the lines in the paper from Vojáček et al. (2015) was conducted by a comparison of the line position of the measured emission line with appropriate emission line databases from Borovicka (1994).

In the present publication, an attempt is presented to utilize PARADE for the analysis of meteor spectra. After a description of the PARADE spectra modeling approach, the extension of the database is discussed. First results are presented by showing some comparisons of PARADE simulations to measured meteorite ablation spectra in ground testing facilities. Results pertain mostly to atomic line emissions. The molecular radiation simulation is tested applying PARADE simulations to observed spectra from the re-entries of WT1190F and CYGNUS OA6. These observed entries provide test cases for the comparison of molecular radiation (Jenniskens et al. 2016; Loehle et al. 2017b).

The object WT1190F was a piece of space debris which returned to Earth on an eccentric orbit with an entry speed of 10.61 km s^{-1} at an entry angle of 20.6∘ (Jenniskens et al. 2016). These entry conditions are more similar to asteroid impacts than most usual space debris impacts from typically low Earth orbits. The object was identified on October 3, 2015 only about 5 weeks prior to the Earth entry on November 13, 2015. The International Astronomical Center in Abu Dhabi and the United Arab Emirates Space Agency deployed an instrumented business jet of type Gulfstream G450 for the observation of the daytime re-entry over the Indian Ocean, south of Sri Lanka. With ESA support, a team from the High Enthalpy Flow Diagnostics Group (HEFDiG) participated in this observation. The entry

was successfully observed with a main fragmentation occurring at an altitude of 56 km. Due to the daytime re-entry condition, the spectral data acquisition was challenging. The data sets allowed for the identification of TiO, which serves as a test case for the diatomic molecular simulations in this article.

The second re-entry used in the present study, CYGNUS OA6, was the resupply spacecraft to the International Space Station operated by Orbital ATK. It was equipped with the Re-Entry Breakup Recorder (REBR) originally foreseen for the entry of the European resupply spacecraft ATV-5. Since the ATV-5 re-entry had to be modified due to onboard power problems, the REBR was not deployed on the ATV-5, but installed in the CYGNUS OA6 spacecraft. The CYGNUS re-entry was a controlled, shallow re-entry over the South Pacific Ocean Uninhabited Area (SPOUA). The re-entry observation started out of Sydney, Australia, where a Bombardier Global Express aircraft was equipped with 13 instruments (http://atv5.seti.org/cygnus/). A team from HEFDiG participated with an Echelle spectrometer. The aircraft was flown to Christchurch, New Zealand, the day before the observation with the possibility to test the equipment. The re-entry occurred as planned on June 23, 2016. The entry interface, that is, when the object reaches an altitude of 120 km, was predicted for 13:21:41 UTC. Aboard the aircraft, the spacecraft was first detected at 13:27:41 UTC just above the horizon. The whole re-entry flight until an altitude of 42 km was successfully observed including some spectral data sets. Atom lines of lithium, sodium, and magnesium are identified along with molecular band radiation of aluminum oxide (AlO). These data sets are used for applying the newly implemented AlO emission in PARADE.

EMISSION SIMULATION AND PLASMA RADIATION DATABASE (PARADE)

The plasma radiation database PARADE has been under development since the early 1990s. The development is funded by ESA and was motivated by the requirement to provide the European community with a tool which does not rely on US simulation codes. The main development was shared between the UK company Fluid Gravity Engineering (FGE) who host the code and the Institute of Space Systems (IRS) at the University of Stuttgart, Germany. The latest version is V3.2.1. The software manual contains a detailed description of the physical background and the software implementation (Smith et al. 2006).

In the software PARADE, a transition is calculated line by line. The radiating medium is assumed to be optically thin. Every single line center wavelength of a transition as well as the intensity of each line are calculated. The intensity profile is calculated by applying a Voigt profile function. Atoms are calculated first, followed by the molecules (Smith et al. 2006).

The species to be calculated are defined in an input file to PARADE. In this input file, the electronic, translational, vibrational, and rotational temperatures have to be defined for each species. Thermal and chemical nonequilibrium can be defined by choosing the temperatures and number densities accordingly.

For the calculation of the radiating line, the program relies on separate input data files containing the spectroscopic constants for each species. Therefore, the extension of the database for meteor spectra as presented in this work concentrates on the compilation of the spectroscopic constants in a format suitable for use in the PARADE code.

The main species included so far are those required for the simulation of atmospheric entry plasma radiation in the atmosphere of Earth, Mars, and the Saturn moon Titan. More recently, effort was put into the development and understanding of nonequilibrium radiation (Joiner et al. 2015). Many two-atomic molecules were implemented, as well as CO2 as a three-atomic molecule (Liebhart et al. 2012).

Alongside the calculation of spectra, the input file features the option to interface with radiation transport codes and computational fluid dynamics codes (Fertig and Herdrich 2009).

Physical Background

In this section, we give a brief description of the physical principles. Generally, the modeling of the radiative emission of gas species is done by calculating the line center wavelength (i.e., the center wavelength) and the line intensity and distribution, that is, the line profile. A detailed description of the theoretical approach can be found, for example, in the fundamental books of Herzberg (1945, 1950).

The position of an emission (or absorption) line is defined by the energy gap between the two internal energy levels involved.

$$\Delta E = Eu - El = h\nu \tag{1}$$

The energies of the involved upper and lower level, *Eu* and *El,* respectively, are calculated based on species-dependent physical constants resulting in the energy of the photon $h\nu$, with the Planck constant h and the frequency in vacuum of the emitted (or absorbed) photon ν. Most of the constants are taken from the NIST database (National Institute of Standards and Technology 2014). The energy levels of atoms are

defined by the electron configuration. Therefore, only electronic transitions exist. For molecules, vibration and rotation of the nuclei are additional degrees of freedom resulting in additional radiative transitions. In the PARADE software, the Born–Oppenheimer approximation is applied so that electronic, vibrational, and rotational transitions can be calculated separately and superposed afterward. Thus, the energy of a rovibronic state of a molecule is

$$E = hc[T_e + G(v) + F(v,J)] \tag{2}$$

with the vacuum speed of light c, the electronic energy term T_e, and the respective vibrational and rotational contribution $G(v)$ and $F(v, J)$ depending on the vibrational quantum number v and rotational quantum number J: The vibrational energy and the rotational energy are calculated from the series expansion.

$$G(v) = \omega_e(v+0.5) - \omega_e x_e(v+0.5)^2 + \omega_e y_e(v+0.5)^3 - \omega_e z_e(v+0.5)^4 + \ldots \tag{3}$$

and

$$F(v,J) = B_v J(J+1)^2 - D_v J(J+1)^2 + \ldots. \tag{4}$$

The constants ωe, xe, ye, ze are so-called spectroscopic constants and are taken from the NIST database. The constants Bv and Dv are constants that take into account that the vibration influences the rotation. They are calculated from the vibrational quantum number v as

$$B_v = B_e - \alpha_e(v+0.5) + \gamma_e(v+0.5)^2 + \ldots \tag{5}$$

$$D_v = D_e + \beta_e(v+0.5) + \delta_e(v+0.5)^2 + \ldots. \tag{6}$$

Again, Be, αe, γe, De, βe, and δe are spectroscopic constants taken from the NIST database.

Depending on different selection rules, which are rules defining whether a transition between two levels of a certain electronic configuration is possible, the line center wavelength of a transition can be calculated. For each electronic state, there are potentially multiple possible vibrational states that can each contain several rotational levels. The rotational lines are spectrally very close to each other and often cannot be resolved in spectroscopic measurements.

In case of emission, the line intensity is the emitted power of the transition in the form of

$$I = A_{ul} h\nu_{ul} N_u, \tag{7}$$

with the Einstein coefficient for the spontaneous emission A_{ul}, the transition energy $h\nu_{ul}$, and the number of the species in the upper state Nu. The Einstein coefficient of spontaneous emission is a measure for the probability that a transition occurs and is calculated with

$$A_{ul} = \frac{16\pi^3 \nu^3}{3E_0 h c^3 |(\psi_u|\mu(r)|\psi_l)^2} \tag{8}$$

where E_0 is the vacuum permittivity, c the vacuum speed of light, ψ_u and ψ_l the wave functions of the upper (u) and the lower (l) level, and $\mu(r)$ the dipole moment of the considered transition. This formulation includes all degenerate sublevels.

For molecules, the transition moment is simplified when the Born–Oppenheimer approximation is applied and the Einstein coefficient becomes

$$A_{ul} = \frac{16\pi^3 \nu^3 q_{V^I - V^{II}} |R_e|^2 S_{J^I - J^{II}}}{3E_0 h c^3 (2J^I + 1)} \tag{9}$$

The double primed values denote the lower and the primed values the upper state. The electronic transition moment R_e (r) considers only the electronic transition.

$$R_e(r) = \left(\psi_{el}^{I} | \mu(r) | \psi_{el}^{II}\right). \tag{10}$$

The vibrational part of the transition is accounted for with the so-called Franck–Condon factor.

$$q_{V^I - V^{II}} = |(\psi_{V^I}|\psi_{V^{II}})|^2. \tag{11}$$

Finally, the rotational part of the transition are the Hönl–London factors $S_{JII}^{\Delta J}$. Depending on the considered rotational band, these factors are calculated for the allowed rotational transitions (Kovacs 1969).

The modeling of diatomic molecules in PARADE requires a detailed database for the electronic transition moment and Franck–Condon factors. For a very simple first interpretation of molecular spectra, we have developed a very simple model for the radiation simulation of diatomic molecular band radiation, which allows a very quick calculation of molecular band radiation if a detailed modeling with PARADE is not available due to, for example, a missing molecular database. The line center wavelengths are calculated according to Equation (1) using Equation (2). Under the assumption of thermal equilibrium, vibrational (and rotational) bands are Boltzmann distributed. Thus, the band intensity distribution, without considering any particular line profile, can be calculated using a Boltzmann distribution function, that is,

$$\frac{N_j}{N} = \frac{hc\,B_{v,u}}{kT}(2J+1)e^{\left(-B_{v,u}\left(J(J+1)\frac{hc}{kT}\right)\right)}. \quad (12)$$

Equation (12) has to be applied for each vibrational band, that is, it considers only rotational energy levels. Using the detailed PARADE code with constant temperatures $T = T_{el} = T_{rot} = T_{vib}$, the qualitative distribution of the intensity yield similar results.

Extension to PARADE

Atoms only have electronic transitions resulting in discrete lines. Depending on the electron configuration of the atom and the selection rules, the number of lines differs between species. Figure 2 shows most of the newly implemented atoms and for comparison a meteorite spectral data set (denoted EM132 in Fig. 2) from measurements recently conducted in the plasma wind tunnel facility PWK1 at University of Stuttgart (Loehle et al. 2017a). The tested fragment was an H chondrite.

The two molecules AlO and TiO were newly implemented. For TiO, the two electronic transitions C-X and A-X were considered due to their high intensity in the visible range. For AlO, the B-X transition was implemented.

The PARADE code was developed for the investigation of Earth re-entries. Some extensions enabled the entry problem of the Huygens capsule in the atmosphere of Saturn's moon Titan to be analyzed. More recently, CO_2 simulations for the entry into the Martian atmosphere were appended (Liebhart et al. 2012). Therefore, air species (O, N, N_2, O_2, and their ions) as well as carbon species (C, CO, CO_2, CH, CN, C_2) are already implemented. The main radiating species to be considered for meteoritic entry were taken from previous publications (Borovicka 1994; Jenniskens 2007; Borovicka and Berezhnoy 2016).

The species in Table 1 were identified to be of primary importance. The species in parentheses were not implemented within this study, but are to be considered for a next phase of the project.

AlO was implemented using previously published spectral data (Londhe et al. 2010; Sriramachandran et al. 2013).

The simulation of TiO was realized using physical constants from the NIST database and literature data from various articles (see Prasad 1962; Phillips 1973; Collins and Fay 1974; Rauh and Ackermann 1974; Hildenbrand 1976; Bell et al. 1979; Barnes et al. 1996; Langhoff 1997; Schwenke 1998; Ram et al. 1999). The radiation of TiO has an important role in astrophysics (Langhoff 1997), and besides the interest in meteor research, TiO is of importance when the observation of re-entries of space structures is considered (Jenniskens et al. 2016).

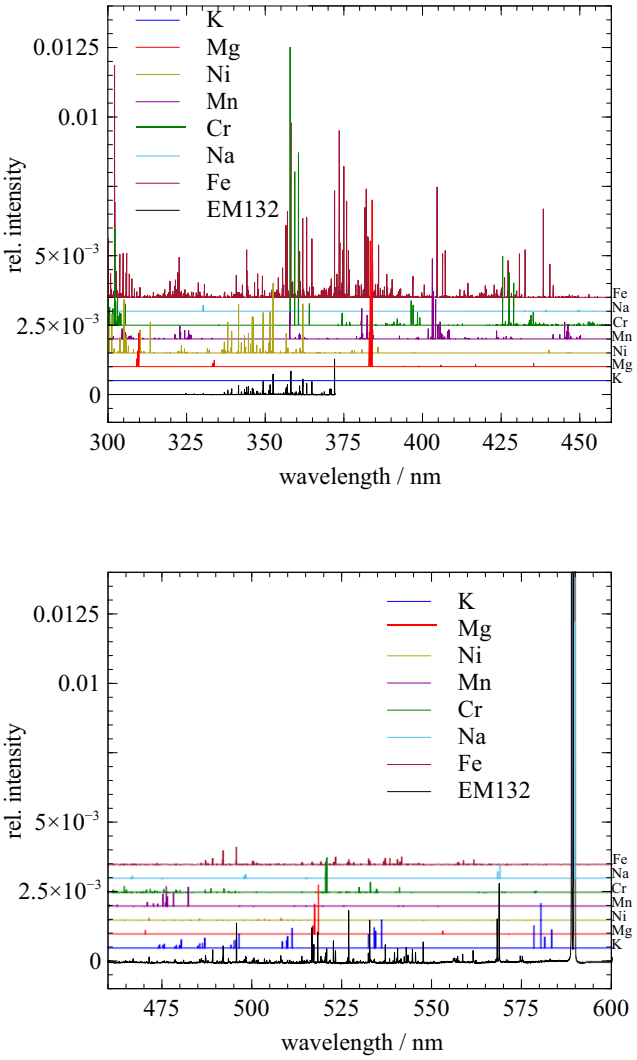

Fig. 2. Parade simulation of atoms and comparison to data from plasma wind tunnel testing (Loehle et al. 2017a; left: 300–460 nm, right: 460–600 nm, simulated atoms shifted). (Color figure can be viewed at wileyonlinelibrary.com.)

RESULTS

Atoms

Figure 2 shows a comparison of PARADE simulations of the newly implemented species and a measured meteoroid spectra from ground testing (Loehle et al. 2017b). An excitation temperature of 10,000 K was assumed. The simulated spectra are then

Table 1. Elements to be included in the PARADE database for meteor entry analysis.

Atoms	Na	K	Ti	V	Cr	Mn	Fe	Ca	Ni	Co	Li	Mg	Si
Molecules	AlO	TiO (MgO	FeO	CaO)									

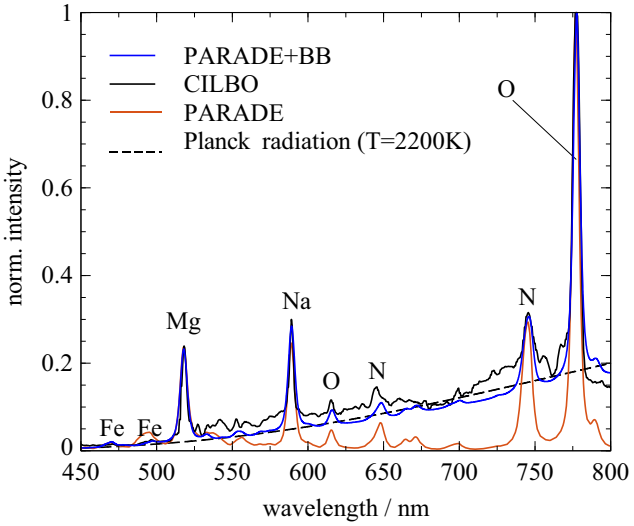

Fig. 3. Comparison of PARADE spectra of single atoms and its superposition to a measured event from the CILBO observatory (Boltzmann excitation temperature of 10,000 K). (Color figure can be viewed at wileyonlinelibrary.com.)

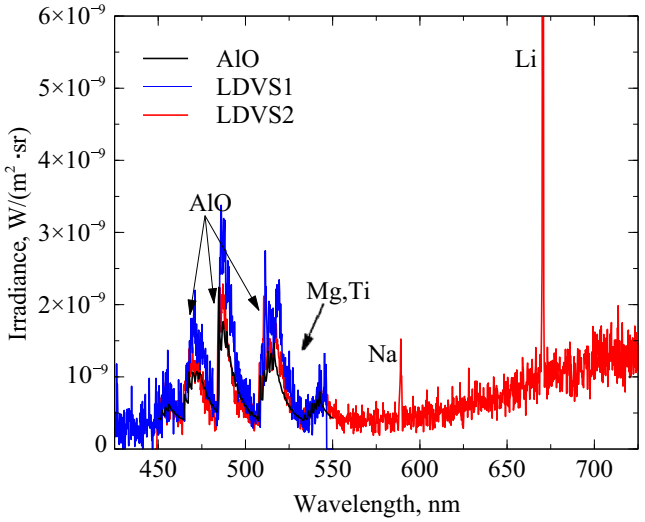

Fig. 4. Flight data from the CYGNUS OA6 observation with the identified spectral contributions (Loehle et al. 2017b). Flight altitude is approximately 70 km. (Color figure can be viewed at wileyonlinelibrary.com.)

Table 2. Abundances of neutral atoms relative to Mg for the spectra measured with CILBO and the observed CYGNUS OA6 entry.

Sample	Mg	O	N	Na	K	Fe	Ni	Mn	Cr	Li	T_{BB}
CILBO	1	1.482×10^4	4.21×10^4	0.11	n/a	2.18	n/a	n/a	0.0422	n/a	2200 K
CYGNUS	1	n/a	n/a	0.86	n/a	n/a	n/a	n/a	n/a	2.15	1500 K

scaled so that in each species, all simulated lines are visible. Figure 2 thus shows if the species seen in the ground testing are covered by the simulation. Although the Echelle spectra have a comparably high wavelength resolution, it is not sufficient to analyze the line profile in more detail. As can be seen, the PARADE simulations cover the prominent lines of K, Mg, Ni, Mn, Cr, Na, and Fe (Fig. 3). The line center wavelengths are in good agreement with the measurement. For potassium (K), the strong lines around 580 nm are not seen in the experiment. There is a large number of lines for Fe, but not all of these lines are seen in the plasma wind tunnel experiment. Borovicka identifies the FeI-15 multiplet ($c^3P \rightarrow x^5P$ -transition) around 527–546 nm to be the most prominent in meteor spectra (Borovicka 1994). The relative intensity distribution in the sodium lines at 567 and 589 nm is very different between simulation and ground test measurement. The 567 nm line is much brighter in the ground testing.

As a second example, we have analyzed one single spectrum observed by the CILBO system. The spectrum shown in Fig. 1 is the raw data without correction for detector sensitivity. However, the detector sensitivity is given and the data can be corrected accordingly, which is shown in Fig. 4. The calibrated spectrum contains a Planck background at a temperature of 2200 K. The spectrum was then simulated using the extended PARADE database as described in the previous sections using the species as indicated in Fig. 4 at a temperature of 10,000 K. The line broadening was assumed with 1.6 nm each for Gaussian and Lorentzian broadening. This corresponds to the nominal instrumental broadening of the spectrometer instrument. It was found that the emission spectra contain Fe, Mg, Na and the air species of atomic

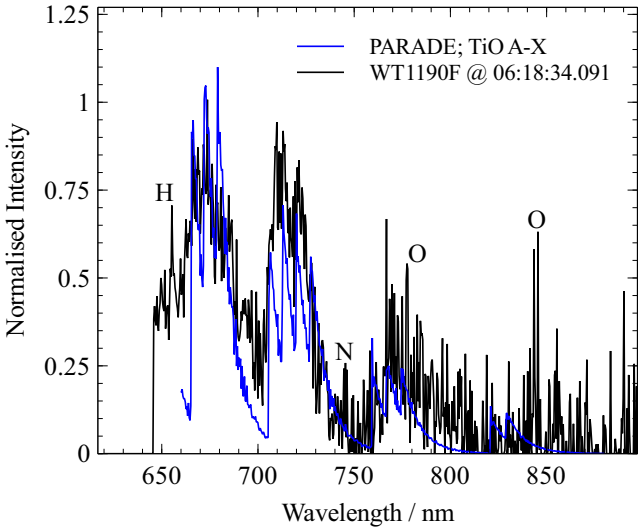

Fig. 5. PARADE simulation of TiO and comparison to vibrational band simulation (vibrational temperature T_{vib} = 4000 K). (Color figure can be viewed at wileyonlinelibrary.com.)

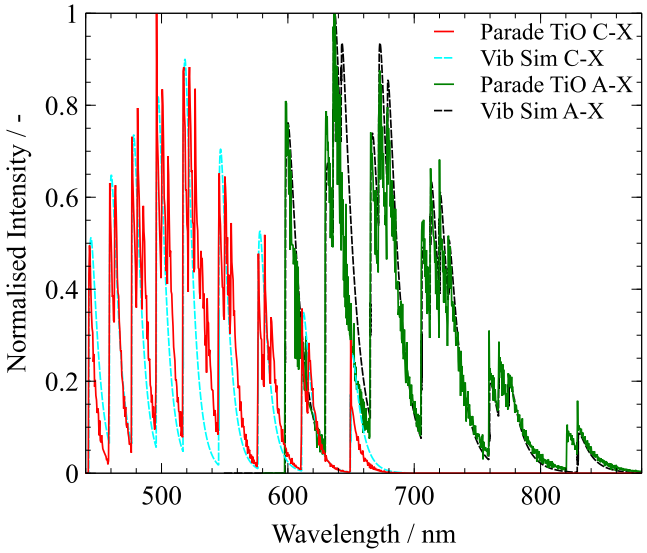

Fig. 6. Comparison of a spectrum measured during the WT1190F entry observation and a spectrum simulated using PARADE (T_{vib} = 8430 K, T_{rot} = 3733 K). Flight altitude is approximately 40 km. (Color figure can be viewed at wileyonlinelibrary.com.)

oxygen and nitrogen. Ionized species were not identified from this particular event, although Na can be easily ionized under meteoroid entry conditions. Borovicka (1994) found that typical meteor spectra are composed of two spectra of almost identical chemical composition at two temperatures, 4000 K and 10,000 K. In the present simulation, a distinction between the two components was not realized.

Table 2 shows a comparison of the atomic abundances relative to Mg for the data from CILBO and the CYGNUS OA6 observation.

Molecules

Figure 5 shows an exemplary TiO spectrum calculated with the new database. For comparison, the mentioned simple calculation of diatomic molecular band radiation is plotted. Good agreement is found between the two methods.

A second set of data was implemented for AlO. This species, as well as TiO, is also of interest for re-entry break-up purposes, as satellite structures are typically made of titanium and aluminum alloys. These alloys then melt and radiate during entry (Jenniskens et al. 2016; Loehle et al. 2017b).

Figure 4 shows a measurement from the CYGNUS OA6 observation and the identified spectral features. In the wavelength interval 450–550 nm, some AlO bands are observed.

Although more experimental data for further validation of the added species are always desirable, their implementation can be considered a success due to the good agreement with the experimental data that is presently available.

DISCUSSION

The newly implemented molecular species were compared to flight data from the observation of WT1190F and CYGNUS-OA6. Furthermore, the vibrational band shape of the PARADE simulations was compared to the simple band shape simulation. The PARADE simulation is a detailed line-by-line calculation of each rovibronic line. For both simulations, the irradiances have been scaled to allow a comparison of the vibrational band shapes with the measured data and a comparison to the rotational line resolution for PARADE. The temperatures are determined through a least squares fitting routine varying the rotational and vibrational temperatures to match the radiative emission.

The TiO molecule was found in the observation of WT1190F. Figure 6 shows the comparison of the flight data with a PARADE simulation. The least squares fitting using PARADE results in a rotational temperature of 3730 K. The vibrational temperature fitted is 8430 K. The plot shows that the simulation agrees well with the measured spectra. It is assumed that the molecule results from a recombination of structural titanium with hot oxygen of the plasma flow leading to such temperatures. The temperature of the solid titanium is significantly lower, probably near the

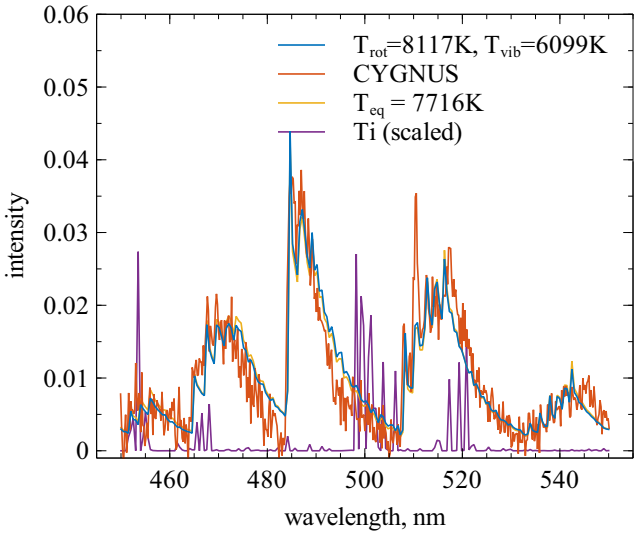

Fig. 7. PARADE simulation of AlO with T_{rot} = 8117 K and T_{vib} = 6099 K. Additionally, titanium lines in this wavelength interval are indicated. PARADE simulation with thermal equilibrium results in $T_{rot} = T_{vib}$ = 7716 K. (Color figure can be viewed at wileyonlinelibrary.com.)

melting point around 2000 K as it was measured during the observation of the ATV-1 re-entry (Loehle et al. 2011).

PARADE simulations of AlO were fitted to CYGNUS OA6 flight data. Shown in Fig. 7, five different bands can be identified. The bands with heads around 450 and 550 nm are weaker than the central bands.

Fitting both vibrational and rotational temperatures simultaneously using PARADE simulations of AlO to the observational data, the resulting temperatures are T_{rot} = 8117 K and T_{vib} = 6099 K (see Fig. 7). For all fits, the Matlab function *nlinfit* was applied. The bands agree well with the measured data from the airborne observation. An equilibrium ($T_{rot} = T_{vib}$) assumption results in T = 7716 K. Taking the sensitivity of the temperatures at these wavelength resolutions and the signal-to-noise ratio into account, the measured temperatures can be assumed to be in equilibrium. There are some titanium atomic lines (see Fig. 7) within the bands of AlO. However, these lines do not seem to disturb the band radiation considerably. For low Earth orbit re-entry, thermal equilibrium between T_{vib} and T_{rot} is not a common feature, especially at this altitude. However, the AlO radiation in this shallow slow re-entry case is resulting from the recombination of a comparably cold aluminum structure with the hot atomic oxygen. This might be an indicator for lower vibrational temperatures.

The simulation of atomic and molecular radiation using the PARADE software with the newly implemented species allows interesting comparisons to observed spectra. If the experimental local emission coefficient is available, these simulations even allow the determination of the species' abundances (Loehle et al. 2010). Furthermore, with these simulations, comparisons between measurements from different observatories and ground testing can be assessed with respect to meteoroid entry physics.

SUMMARY AND OUTLOOK

This article presents some extensions to ESA's PARADE database for the simulation of emission spectra as occurring during meteoroid flights and re-entry break-up of man-made structures. The implementation of atoms of interest agrees well with recently acquired plasma wind tunnel data. Measured meteor spectra using the CILBO ICC8 camera have been interpreted using PARADE. In addition, the molecular data agree well with the airborne flight observation data for the CYGNUS OA6 re-entry in 2016 as well as the WT1190F entry in 2015.

The PARADE database is going to be extended further as required for the analysis of meteoroid entries. Furthermore, there are additional experimental campaigns ongoing for the observation of meteoroid entries and for the investigation of meteorites in the ground testing facilities at IRS, which will be used to improve the molecular radiation modeling in PARADE. One requirement is to implement additional diatomic species (MgO, FeO, CaO) in order to analyze the molecular radiation of prominent species of meteoroid radiation during entry.

PARADE is programmed for the simulation of very high resolution spectra. Thus, an improvement in the resolution of observed spectral data directly allows for better spectral analysis through PARADE. For example, the application of Echelle spectrometer for the flight observation will enable the acquisition of highly resolved spectra. With the results of the PARADE extension presented in this study, simulated spectra will give more insight during upcoming entry observations or ground testing attempts. The recently started analysis of meteoroid entry spectra in ground testing facilities benefits from the new PARADE simulation capabilities. Improved spectral analysis will allow the provision of better spectral data in order to assess meteoroid entry physics.

Acknowledgments—The support of the European Space Agency under contract No. 5001019152 is greatly appreciated. The funding of the HEFDiG for the participation in the observation campaigns by ESA's Space Debris Office is gratefully acknowledged. As

required by the instructions for authors for *Meteoritics & Planetary Science*, no conflict of interest has to be declared. Open Access funding enabled and organized by ProjektDEAL.

Editorial Handling—Dr. Josep M. Trigo-Rodríguez

REFERENCES

Barnes M., Merer A. J., and Metha G. F. 1996. Rotational and hyperfine structure of some low-j lines in the a3phi - x3delta(0, 0) band of TiO. *Journal of Molecular Spectroscopy* 180:437–440. https://doi.org/10.1006/jmsp.1996.0269

Bell R. A., Dwivedi P. H., Branch D., and Huffaker J. N. 1979. Rotational dependence of Franck-Condon factors for selected band systems of TiO, ZrO, MgO, LaO, and SiO. *The Astrophysical Journal Supplement Series* 41:593. https://doi.org/10.1086/190632.

Borovicka J. 1994. Two components in meteor spectra. *Planetary and Space Science* 42:145–150. https://doi.org/10.1016/0032-0633(94)90025-6

Borovicka J. and Berezhnoy A. A. 2016. Radiation of molecules in benesov bolide spectra. *Icarus* 278:248–265. https://doi.org/10.1016/j.icarus.2016.06.022

Ceplecha Z., Borovicka J., Graham Elford W., ReVelle D. O., Hawkes R. L., Porubčan V., and Šimek M. 1998. Meteor phenomena and bodies. *Space Science Reviews* 84:327–471. https://doi.org/10.1023/a:1005069928850.

Colas F., Zanda B., Vaubaillon J., Bouley S., Marmo C., Audureau Y., Kwon M. K., Rault J. L., Caminade S., Vernazza P., Gattacceca J., Birlan M., Maquet L., Egal A., Rotaru M., Birnbaum C., Cochard F., and Thizy O. 2015. French fireball network fripon. In *Proceedings of the IMC*. Mistelbach, Austria: International Meteor Organization. pp. 37–40.

Collins J. G. and Fay T. D. 1974. Radiative opacities for the alpha, gamma, and phi systems of titanium monoxide. *Journal of Quantitative Spectroscopy and Radiative Transfer* 14:1259–1272. https://doi.org/10.1016/0022-4073(74)90094-6

Fertig M. and Herdrich G. 2009. The advanced Uranus Navier-Stokes code for the simulation of nonequilibrium re-entry flows. *Transactions of the Japan Society for Aeronautical and Space Sciences, Space Technology Japan*, 7(ISTS26):Pe_15–Pe_24. https://doi.org/10.2322/tstj.7.pe15

Golub A. P., Kosarev I. B., Nemchinov I. V., and Shuvalov V. V. 1996. Emission and albation of a large meteoroid in the course of its motion through the Earth's atmosphere. *Solar System Research* 30:183–197.

Herzberg G. 1945. *Atomic spectra and atomic structure*. New York: Dover Publications.

Herzberg G. 1950. *Molecular spectra and molecular structure, Vol. 1: Spectra of diatomic molecules*. New York: Dover Publications.

Hildenbrand D. L. 1976. Mass spectrometric studies of the thermochemistry of gaseous TiO and TiO_2. *Chemical Physics Letters* 44:281–284. https://doi.org/10.1016/0009-2614(76)80510-6

Jenniskens P. 2006. *Meteor showers and their parent comets*. Cambridge: Cambridge University Press.

Jenniskens P. 2007. Quantitative meteor spectroscopy: Elemental abundances. *Advances in Space Research* 39:491–512. https://doi.org/10.1016/j.asr.2007.03.040

Jenniskens P. 2017. Meteor showers in review. *Planetary and Space Science* 143:116–124. https://doi.org/10.1016/j.pss.2017.01.008

Jenniskens P., Albers J., Koop M., Odeh M., Al-Noimy K., Al-Remeithi K., Al Hasmi K., Dantowitz R. F., Gasdia F., Loehle S., Zander F., Hermann T., Farnocchia D., Chesley S. R., Chodas P. W., Park R. S., Giorgini J. D., Gray W. J., Robertson D. K., and Lips T. 2016. Airborne observations of an asteroid entry for high fidelity modeling: Space debris object wt1190f. https://doi.org/10.2514/6.2016-0999

Joiner N., Beck J., Capitelli M., Fertig M., Herdrich G., Laricchiuta A., Liebhart H., Lino da Silva M., Ngyen-Bui N. T. H., Reynier P., and Tran P. 2015. Validation of aerothermal chemistry models for re-entry applications: Theoretical and computational synthesis. 8th European Symposium on Aerothermodynamics. ESA.

Koschny D., Bettonvil F., Licandro J., Luijt C. V. D., Mc Auliffe J., Smit H., Svedhem H., de Wit F., Witasse O., and Zender J. 2013. A double-station meteor camera set-up in the Canary Islands CILBO. *Geoscientific Instrumentation, Methods and Data Systems* 2:339–348. https://doi.org/10.5194/gi-2-339-2013.

Kovacs I. 1969. *Rotational structure in the spectra of diatomic molecule*. Budapest: Akademiai Kiado.

Langhoff S. R. 1997. Theoretical study of the spectroscopy of TiO. *The Astrophysical Journal* 481:1007–1015. https://doi.org/10.1086/304077

Liebhart H., Bauder U., Herdrich G., Fasoulas S., and Röser H.-P. 2012. Numerical modeling of radiative and convective heat flux for entry flights in CO_2 containing atmospheres. Fluid dynamics and co-located conferences. https://doi.org/10.2514/6.2012-3195

Loehle S., Lein S., Eichhorn C., Herdrich G., and Winter M. W. 2010. Spectroscopic investigation of an inductively heated CO_2 plasma for mars entry simulation. *Journal of Technical Physics* 50:151–164.

Loehle S., Marynowski T., Knapp A., Wernitz R., and Lips T. 2011. Analysis of the ATV1 re-entry using near-UV spectroscopic data from the NASA/ESA multi-instrument aircraft observation campaign. In 7th ESA Aerothermodynamics Symposium for Space Vehicles. ESA.

Loehle S., Zander F., Hermann T., Eberhart M., Meindl A., Oefele R., Vaubaillon J., Colas F., Vernazza P., Drouard A., and Gattacceca J. 2017a. Experimental simulation of meteorite ablation during earth entry using a plasma wind tunnel. *Astrophysical Journal* 837:112.

Loehle S., Zander F., Lemmens S., and Krag H. 2017b. Airborne observations of re-entry break-up: Results and prospects. In 7th European Conference on Space Debris, Darmstadt, Germany, ESA.

Londhe C. T., Sunanda K., Saksena M. D., and Behere S. H. 2010. Franck-condon factors and r-centroids of B–X, C–X and C–A band systems of AlO molecule. *Journal of Molecular Spectroscopy* 263:178–182. https://doi.org/10.1016/j.jms.2010.07.013

Millman P. 1932. An analysis of meteor spectra. *Annals of the Astronomical Observatory of Harvard College* 82:113–147.

National Institute of Standards and Technology. 2014. Atomic Spectra Database. http://physics.nist.gov/PhysRefData/ASD

Oepik E. 1958. *Physics of meteor flight in the atmosphere*. London, GB: Interscience Publishers.

Phillips J. G. 1973. Molecular constants of the TiO molecule. *The Astrophysical Journal Supplement Series* 26:313. https://doi.org/10.1086/190283

Prasad S. S. 1962. Franck-Condon factors and r-centroids for the a-system of TiO. *Proceedings of the Physical Society* 79:1078–1079. https://doi.org/10.1088/0370-1328/79/5/121

Ram R. S., Bernath P. F., Dulick M., and Wallace L. 1999. The a3phi-x3delta system (gamma bands) of TiO: Laboratory and sunspot measurements. *The Astrophysical Journal Supplement Series* 122:331.

Rauh E. G. and Ackermann R. J. 1974. First ionization potentials of some refractory oxide vapors. *Journal of Chemical Physics* 60:1396–1400. https://doi.org/10.1063/1.1681210

Schwenke D. W. 1998. Opacity of TiO from a coupled electronic state calculation parametrized by ab initio and experimental data. *Faraday Discussions* 109:321–334. https://doi.org/10.1039/a800070k

Smith A. J., Wood A., Dubois J., Fertig M., and Pfeiffer B. 2006. Plasma radiation database parade v2.2. Technical Report TR28/96 Issue 3. Emsworth, UK: Fluid Gravity Engineering Ltd.

Sriramachandran P., Viswanathan B., and Shanmugavel R. 2013. Occurrence of AlO molecular lines in sunspot umbral spectra. *Solar Physics* 286:315–326. https://doi.org/10.1007/s11207-013-0264-1

Vojáček V., Borovicka J., Koten P., Spurný P., and Štork R. 2015. Catalogue of representative meteor spectra. *Astronomy & Astrophysics* 580:A67. https://doi.org/10.1051/0004-6361/201425047